JOURNAL OF PROPULSION AND POWER
Vol. 10, No. 5, Sept.–Oct. 1994

Compressor Unsteady Aerodynamic Response to Rotating Stall and Surge Excitations

Kuk H. Kim* and Sanford Fleeter†
Purdue University, West Lafayette, Indiana 47907

A series of experiments are performed in an extensively instrumented three-stage axial flow research compressor to investigate the fundamental aeromechanics of compressor flow instabilities, including pure rotating stall, classic surge, and the stable modified surge flow regimes between these two modes. In particular, the flow-induced vibration forcing functions together with the resulting blade row unsteady aerodynamic response generated by these various compressor flow instabilities are measured with a rotating cross hot-wire, with the resulting blade row gust response measured with dynamic pressure transducers embedded in the first-stage rotor blading. The forcing function data are analyzed in terms of the streamwise and transverse gust components and the mean rotor relative velocity, with the unsteady rotor blade row gust response specified by the unsteady lift response to each instability mode. The data show that rotating stall excites a relatively constant rotor blade response, approximately 27% of the steady loading. Surge excites an unsteady response proportional to the level of surge present in the instability mode, thereby increasing as the *B* parameter increases. However, the absolute level of the response resulting from surge is considerably less than the rotating stall generated response, approximately 37–67%.

Nomenclature

A_c = compressor equivalent flow area
a = speed of sound
B = compressor instability mode parameter
F = frequency
f_c = rotating stall cell frequency
f_{ex} = frequency of excitation relative to the rotor
f_r = rotor rotational frequency, 37.5 Hz
L_c = compressor equivalent length
N_r = number of rotor blades (43)
N_{rev} = number of data points per rotor revolution
N_s = number of blade spacings from the reference (1st) blade
T_c = rotating stall cell period
T_{sp} = specified time period for one cycle of rotating stall propagation
U = midspan rotor speed
u^+ = first harmonic streamwise gust velocity
V_p = compressor volume
V_x = axial velocity
V_x^+ = first harmonic unsteady axial velocity
v^+ = first harmonic transverse gust velocity
W = mean rotor relative velocity
$\bar{\alpha}$ = mean absolute flow angle
$\bar{\beta}$ = mean rotor relative flow angle
$\Delta\phi$ = unsteady lift phase change between two successive rotating stall cell cycles

Introduction

COMPRESSORS encounter flow instabilities under certain operating conditions, demarcated on the compressor performance map by the surge line, a barrier that separates regions of stable and unstable operation. The surge line is of particular interest due to its close proximity to the region of compressor maximum pressure rise and efficiency. Current generation turbomachines must allow for a safety margin—the surge margin—that places the operating region far enough removed from the surge line to prevent the onset of instability. Unfortunately, this safety margin moves the compressor operating line away from its maximum efficiency.

The term surge line is somewhat misleading. Two possible phenomena can occur when this boundary is reached, generally categorized as rotating stall or surge. Surge refers to a global oscillation of the mass flow through the compression system, often with complete flow reversal. It is a phenomena of the entire compression system, consisting of the compressor and the system into which it discharges. Rotating stall, in contrast, is an instability local to the compressor itself, and is characterized by a circumferential nonuniform mass deficit that propagates around the compressor annulus at a fraction of rotor speed.

There are two disadvantages associated with a compressor encountering an instability marked by the surge line. First, compressor performance falls drastically when a surge line flow instability is encountered. On flight-rated turbine engines, such a performance degradation and resulting loss of thrust can be catastrophic. Second, the surge line flow instability may be a dangerous unsteady aerodynamic excitation resulting in blade vibrations, as discussed, e.g., in regard to centrifugal compressors by Haupt et al.[1] and Jin et al.[2,3] Thus, rotating stall and surge are flow instabilities that not only limit compressor performance, but also affect their durability.

Blade vibration resulting from rotating stall, although violent, is of very short duration. However, modern high-stage loading designs with low-to-moderate design weight and tip speeds can be life-limited in the number of stalls tolerable. Surge-induced vibration is a self-excited, limit-cycle instability. Excessive vibrational response far over the endurance limit can drastically restrict the number of stalls a compressor may experience without blade fatigue or serious reduction in its normal high-cycle fatigue strength. Thus, the surge instability forced response problem differs from the usual instability problem in that the interest is not the instability boundary, but rather the level of response.

Research on rotating stall and surge has focused on determining their flow characteristics to improve the ability to pre-

Received July 19, 1993; revision received Feb. 15, 1994; accepted for publication March 2, 1994.

*Graduate Research Assistant, School of Mechanical Engineering. Student Member AIAA.

†Professor, Mechanical Engineering, School of Mechanical Engineering. Associate Fellow AIAA.

dict them as well as on their impact on compressor performance. Only minimal fundamental research attention has been directed at the issues of rotating stall and surge flow induced vibrations. In fact, there have been no fundamental unsteady aerodynamic experiments directed at investigating the fundamental surge-line flow instability unsteady aerodynamics as applicable to blade row durability issues. Thus, there is a clear need for fundamental rotating stall and surge forcing function and resulting gust response unsteady aerodynamic data.

In this article, fundamental experiments are performed that investigate surge, rotating stall, and the modified surge instability regimes, including the flow-induced vibration forcing functions generated during these various rotating stall and surge excitations, together with the resulting blade row unsteady aerodynamic response. The various instability forcing functions are measured with a rotating cross hot-wire, with the resulting blade row gust response measured with dynamic pressure transducers embedded in the rotor blade. Specific technical objectives include 1) identification of the compressor flow characteristics during the transition from pure rotating stall to the classic surge instability mode, i.e., with different levels of modified surge; 2) determination of the unsteady aerodynamic forcing function characteristics of rotating stall, surge, and the modified surge instabilities in between; and 3) quantification of the unsteady aerodynamic response of the first-stage rotor blade row to the various rotating stall and surge instability excitation unsteady aerodynamic forcing functions.

The fundamental compressor flow instability is governed by the value of the B parameter defined in Eq. (1). It is the ratio of the pressure or acceleration force to the fluid momentum or inertial force, and characterizes whether the instability mode of a compressor is rotating stall or surge.[4,5] If B is smaller than B_{critical}, the instability mode of the compressor will be rotating stall, with a surge instability mode found for B values larger than B_{critical}. When the value of B is between those corresponding to rotating stall and classic surge or is near B_{critical}, the compressor encounters a modified surge instability. This has the basic characteristics of a surge cycle in that the entire annulus flow fluctuates in the axial direction, but rotating stall persists throughout the surge cycle, during both the blowdown and the recovery phases. Until recently, this instability flow regime had not been recognized as a separate instability flow regime and, hence, had been neglected. The flow characteristics of this transitional flow regime were experimentally studied by Pust,[6] with the post-stall compressor performance computationally investigated by Jun et al.[7] Still, information regarding this region is very limited

$$B = \frac{\frac{1}{2}\rho U^2 A_c}{\rho \omega U L_c A_c} = \frac{U}{2a}\sqrt{\frac{V_p}{A_c L_c}} \tag{1}$$

Research Compressor

These experiments are performed in the Purdue Axial Flow Research Compressor that is extensively instrumented with cross hot-wire probes, steady and dynamic pressure transducers, and endwall microphones. The compressor plenum consists of two sections, first a small connecting section directly attached in line of flow, and the main plenum section that contains a movable wall to generate different compressor volumes and thus compressor instability modes. The throttle plate is motorized with a variable speed control. The overall compressor, compressor volumes, and airfoil characteristics are defined in Table 1.

The occurrence of rotating stall, surge or the transition flow regimes in between is determined by the compressor volume, thereby specifying the value of B, per Table 1. The flow instabilities are generated by operating the compressor at a constant speed of 2250 rpm with the throttle completely open. The throttle is then very slowly closed so as to generate the longest duration of precursor rotating waves[8] until data acquisition is initiated by an analog trigger signal, with the trigger level set to capture the occurrence of rotating stall or surge. The throttle closure rate did not affect the character of rotating stall and surge development or the disturbance magnitudes once the instability was initiated. Unsteady data quantifying the flowfield, the compressor end wall pressures, and the rotor blade surface unsteady pressures are acquired and digitized.

Table 1 Airfoil and compressor characteristics

	IGV	Rotor	Stator
Number of airfoils	36	43	3
Chord C, mm	30	30	30
Solidity	0.96	1.14	1.09
Camber Θ, deg	36.9	28.0	27.7
Stagger angle γ, deg	21.0	36.0	−36.0
Aspect ratio	2.0	2.0	2.0
Thickness/chord, %	10	10	10
Design flow rate, kg/s		2.03	
Design axial velocity, m/s		24.38	
Design rotational speed, rpm		2250	
Number of stages		3	
Hub/tip radius ratio		0.714	
Stage efficiency, %		85	
B-value		Volume, m^3	
0.26		3.4	
0.40		8.5	
0.76		30.04	
L_c, m		2.93	
a, m/s		343.2	
U, m/s		42.5	

Instrumentation

The instability flow regimes are characterized by the time history of the instantaneous axial velocity, the transient rotating stall cell-averaged flow coefficient V_x/U, and the nondimensional pressure rise coefficient $\Delta p/\rho U^2$, where the plenum pressure Δp is referenced to ambient. These data are presented in a time history format, not a compressor map, to relate the forcing function and unsteady lift characteristics to the instability development events.

The compressor unsteady inlet flowfield generating the first-stage rotor blade row unsteady aerodynamic response during rotating stall and surge initiation and development are measured using rotating cross hot-wire probes. Reverse flows, if they exist, are measured with two cross hot-wire probes located at blade midspan (r = 7.087 in.). The two probe orientations, shown in Fig. 1 at their 0-deg incidence positions, provide a flow measurement capability of −40- to 75-deg incidence (10–125 deg) to the rotor blade. The first cross hot-wire probe accurately measures flow angles varying from −40 to +40 deg of incidence (10–90 deg), with the second accurately quantifying flow angles varying from −5 to +75 deg of incidence (45–125 deg). Note that since the hot-wire is measuring the rotor relative velocity, it reads compressor wheel speed U (≈139 ft/s) at zero axial flow velocity. However, rotating stall and surge do induce low relative velocities. Therefore, both cross hot-wire probes are calibrated for velocities from 9.14 m/s (30 ft/s) to 51.8 m/s (170 ft/s), and angles ranging from +45 to −45 deg. The uncertainties in the velocity and the flow angle measurements were determined to be 5% and ±1.0 deg. Centrifugal loading effects on the rotating hot-wire sensor resistance and thus the responses were found to be negligible. Stationary hot-wire calibrations were validated in the rotating frame by Hah and Lakshminarayana.[9] These cross hot-wire probes are both located at the rotor blade midspan (r = 7.087 in.) in positions shown in Fig. 1.

The first-stage rotor blade midspan surface unsteady pressures are measured with 12 ultraminiature, high-response

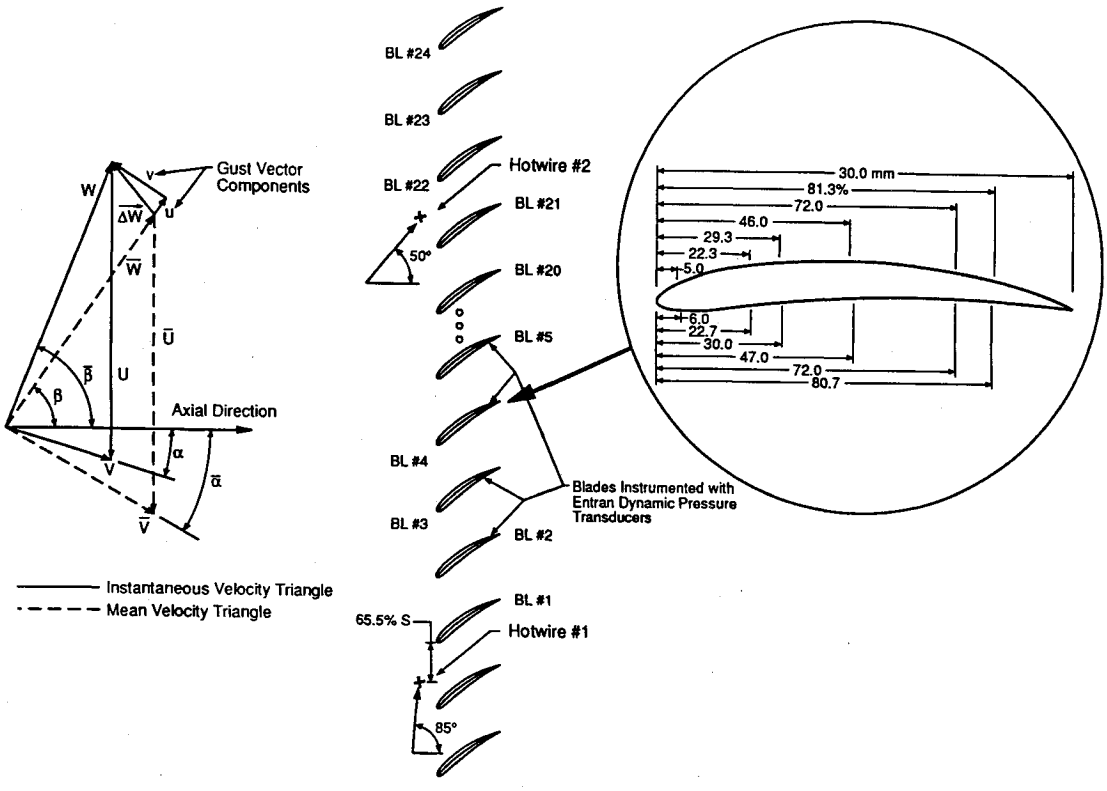

Fig. 1 Rotor instrumentation schematic.

transducers embedded in the rotor blades (Fig. 1). To minimize the possibility of flow disturbances associated with the inability of the transducer diaphragm to exactly maintain the surface curvature of the blade, a reverse mounting technique is utilized. The pressure surface of one blade and the suction surface of the adjacent blade are instrumented, with transducers embedded in the nonmeasurement surface and connected to the measurement surface by a static tap. Since the transducer surface is miniature, the active diameter being 0.060 in., and parallel to the blade surface, the transducers are mounted virtually radial. Thus, the centrifugal field does not act on the transducer active surface, and has a negligible effect on the unsteady pressure measurements. The embedded dynamic transducers are both statically and dynamically calibrated. The static calibrations show good linearity and no discernible hysteresis. The dynamic calibrations demonstrate that the frequency response, in terms of gain attenuation and phase shift, are not affected by the reverse mounting technique. The maximum error in gain and phase angle were determined to be 0.60 dB and 1.5 deg, respectively.

The two rotating cross hot-wire probes and the 12-blade, surface-mounted dynamic pressure transducers are interfaced to the stationary frame-of-reference through a 46-channel, mercury-wetted slip-ring assembly. On-board signal conditioning of the transducer output signals is performed to maintain a good signal-to-noise ratio through the slip rings. The remaining channels of the slip-ring assembly provide excitation to the transducers and other miscellaneous data transfer.

Digital data acquisition is initiated by an analog trigger signal from a single microphone upstream of the first rotor row, with the trigger level set to capture the occurrence of rotating stall or surge while the throttle is very slowly closed. The unsteady flowfield, the blade surface unsteady pressures, and the plenum pressure data are acquired with 2 cross hot-wire probes, 12 dynamic pressure transducers, and a Scanivalve® pressure transducer, respectively, and then digitized. Fifty percent of a 5.5-s data burst is saved pretrigger, with the remainder of the samples post-trigger. Once data acquisition has been completed, the compressor motor is automatically shut down by the computer. A sampling rate of 5000 Hz was chosen to avoid aliasing of the important machine frequencies, i.e., the rotor and inlet guide vane (IGV) blade passing frequencies, 1.3 kHz and 1.6 kHz, respectively.

Before analysis, all unsteady data are filtered to remove high-frequency noise. The hot-wire data are low pass filtered to 100 Hz using a Butterworth filter of order 10, resulting in a response phase lag of approximately 0.5 revolutions. The unsteady pressure response data are bandpass filtered from 0.5 to 100 Hz using a Butterworth band filter of order 2. Since the signals near the low-frequency limit are of significant interest, minimal low-frequency data distortion is desirable. Therefore, the low-order filter is used for the bandpass filtering of the pressure data because the higher order filter produces a longer numerical transient.

Data Analysis

The unsteady velocity field quantifies the characteristics of the instability forcing functions generating the unsteady aerodynamic response of the rotor blade row. However, reverse flows can be a problem. Also, the annulus flow is both time and spatially variant. Greitzer and Day[5,10] avoided the reverse flow measurement problem by using an analytical technique to compute the flow coefficient, with the mass flow determined using a calibrated throttle and a continuity balance in the plenum.

In these experiments, rotating cross hot-wire probes are utilized to measure the velocity, thereby avoiding the reverse flow measurement problem. They enable flows with up to 160 deg in flow angle variation to be measured. Thus, the measured relative velocity is always positive, with reverse flow determined from the flow angle measurement alone. They are set such that reverse flows to 40 deg can be measured.

The unsteady aerodynamic forcing function generating the rotor blade row unsteady aerodynamic response is characterized by the fluctuating velocity in the streamwise and the transverse directions. In particular, the first harmonic of the fluctuating velocity is analyzed, with the frequency of interest being the rotating stall frequency or the surge frequency. Since rotating stall and surge are transient phenomena, the mean flow is a localized mean, the average velocity during a single

cycle of rotating stall or a single cycle of surge. In the presentation of the localized mean rotor relative velocity time history for rotating stall forcing function data, successive rotating stall cycles are averaged. The surge excitation forcing function data acquisition period covers only 2–3 surge cycles. Hence, the average on a single successive surge cycle is performed every few points. The hot-wire data provide the instantaneous W and β from which the mean and fluctuating flowfields are determined. The forcing function, defined by u^+ and v^+, are determined from the u and v gust velocity components, where u and v are the streamwise and transverse gust components and $u = W - \bar{W}\cos(\beta - \bar{\beta})$, $v = W\sin(\beta - \bar{\beta})$.

Transient blade row unsteady pressure response data are necessary at the frequencies of interest. Hence, a Fourier analysis is performed to track the development of the transient event in the frequency domain, and thereby determine the frequency content. However, when appropriate frequency resolution is achieved, time resolution becomes a problem, particularly if the sampling frequency is high. At a sampling speed of 5000 Hz, chosen to avoid aliasing of the rotor blade pass frequency, the resulting surge and rotating stall frequencies are far from the sampling speed and time resolution is difficult.

To avoid these frequency-time resolution tradeoffs, an alternative method is used. First, the important frequencies in the stall and surge transient histories are identified from the data with the Gabor spectrogram, a joint time-frequency analysis technique that avoids the limitations of the short time Fourier transform (STFT) spectrogram by using two elemental techniques, the Gabor transform and the pseudo Wigner-Ville distribution (PWVD).

With the rotating stall frequency with largest magnitude determined, the pressure data from blades other than the first are adjusted to account for the circumferential time lag associated with the transducers being distributed over four blades. Each blade sees the rotating stall at different times. Thus, to determine a blade differential pressure response to rotating stall as if the data were taken with one blade only, the time trace is adjusted by $(N_s/N_r) \times (f_{ex}/f_r) \times N_{rev}$. Note that the surge-generated unsteady pressure data do not have to be time-lag adjusted because surge is a purely axial phenomena.

Finally, a discrete Fourier transform (DFT) is applied to successive cycles of data whose period corresponds to the frequency of interest, e.g., the rotating stall frequency, and the first harmonic analyzed. Since, the number of points in a single cycle of data at the rotating stall frequency is smaller than that necessary for a fast Fourier transform (FFT), the time resolution is significantly improved with this method. One problem is that leakage error is introduced if the frequency of the transient phenomena changes, causing the period of data selected for the DFT to be incorrect for that frequency. A study of DFT leakage showed that for less than 20% variation in frequency, the resulting errors in magnitude and phase are less than 10% and 40 deg, respectively. Fortunately, the maximum rotating stall frequency variation is less than 15% in these experiments, and therefore, the maximum errors in magnitude and phase are expected to be less than 10% and 40 deg. Although these errors are larger than desirable, it is considered to be a worthy tradeoff for the improved time resolution, 20 times better with DFT as compared to FFT.

The unsteady aerodynamic response of the first-stage rotor blade row to the various instabilities are quantified by the unsteady lift, the integral of the unsteady differential pressure across the rotor blade. To compute this, the voltages from the pressure and suction surface transducers are first bandpass filtered from 0.5 to 100 Hz to eliminate high-frequency noise. Then the first harmonic of the unsteady pressures are analyzed by the DFT analysis. Note that since a dimensionless chordwise location is used as the variable of integration, the unsteady lift magnitude is per blade area, and thus, has dimensions of psi. The unsteady lift phase provides time information. In particular, a coherent phase corresponds to a coherent wave, e.g., a rotating stall cell. Also, the phase value indicates whether the frequency selected for the harmonic analysis correctly matches the propagation speed of the physical wave. An incorrect frequency can be due to 1) the characteristic frequency, i.e., rotating stall or surge frequency, changing with time; or 2) the specified frequency chosen for analysis is incorrect. If the frequency is correct, the phase should be constant. However, if the frequency is slightly incorrect, the magnitude data would be correct within the leakage error band and the phase would change by a constant value. Thus, the slope or the change in phase can be used to measure the propagation speed per the following:

$$T_c = [T_{sp}/(1 + \Delta\phi)] \tag{2}$$

If the slope of the unsteady lift phase is negative, the correct frequency is less than the specified frequency. If the slope of the unsteady lift phase is positive, the correct frequency is greater than the specified frequency. Note that the correct speed can only be calculated if no data points are skipped or repeated at each DFT point because skipped or repeated data points will also cause a phase change. Thus, the actual surge frequency could not be calculated since the data did not cover enough surge cycles, and thus, data points were repeated. However, the magnitude data are still accurate within the leakage error bands.

Results and Discussion

The unsteady aerodynamic response of blade rows to rotating stall, surge, and the transitional flow regime between pure rotating stall and classic surge are important with regard to engine durability. Specific technical issues of interest include the rotating stall and surge unsteady aerodynamic forcing functions and the resulting blade row response, i.e., the rotor blade surface unsteady pressure and unsteady lift harmonic magnitude and phase during instability inception and development, the level of the unsteady response, and the differences in this response to rotating stall, surge and modified surge instability excitations. These issues are addressed for the following three different instability modes: $B = 0.26$, 0.40, and 0.76.

Stall Instability Modes

With $B = 0.26$, the compressor enters into rotating stall (Fig. 2a). The axial velocity slowly decreases until about 98 rotor revolutions, where a small stall cell emerges and grows very rapidly to half the steady-state size in less than 5 rotating stall cycles, less than 10 rotor revolutions. Initially, the stall cell size oscillates, but it then grows to its constant size in about 30 rotor revolutions, with the magnitude of the stall cell depth being approximately 75 ft/s in axial velocity. The initial oscillation in the rotating stall cell size is indicative of the damped oscillatory motion that accompanies settlement into a stable equilibrium point. This behavior is exhibited by both the nondimensional pressure rise coefficient and the average flow coefficient. However, since the throttle is continuously being closed, albeit very slowly, the compressor's stalled operating point changes with time.

With $B = 0.40$ (Fig. 2b), the compressor exhibits behavior very different from that of rotating stall alone or surge alone. Analogous to the previous case, initially the axial velocity very slowly decreases as the compressor pressure rise increases toward the peak value, until approximately 103 revolutions, a small stall cell emerges and quickly grows into a full size stall cell depth of 80 ft/s in axial velocity in a little over 10 revolutions. This constitutes the "blowdown" phase of the surge cycle where the pressure in the plenum that had been building to the peak pressure rise point discharges, and the flow in the entire annulus is significantly reduced from

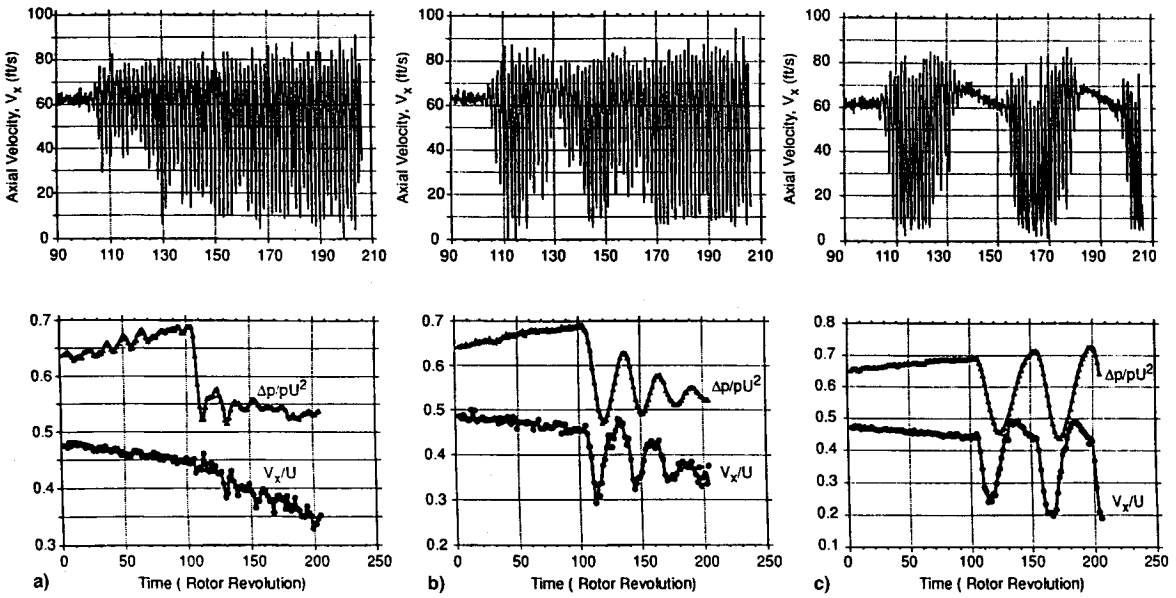

Fig. 2 Instability flow regime characterization: a) pure rotating stall (B = 0.26), b) modified surge close to pure rotating stall (B = 0.40), and c) classic surge (B = 0.76).

the nonstalled value. At approximately 115 rotor revolutions, where the axial velocity reaches its lowest value, the "charging" phase of the surge cycle begins where the plenum pressure starts to rise again. Thus, so far, the compressor behavior exhibited is that of a classic surge cycle in which the entrance into the surge cycle is accompanied by rotating stall. However, the resemblance to the classic surge cycle ends here.

In contrast to the classic surge cycle, rotating stall persists throughout the recovery well into the beginning of the next surge cycle. The rotating stall cell merely gets smaller during the recovery phase and thus, the plenum is no longer able to recharge its pressure to the presurge value, recovering only 60% of the discharged pressure (Fig. 2b). The compressor behavior during the entrance into the second surge cycle is much like the first: the plenum pressure discharges and the stall cell rapidly grows into the full size in approximately 15 rotor revolutions. However, during the recovery phase of the second surge cycle, rotating stall persists so strongly and without much reduction in size that the plenum pressure is only able to recover about 40% of the original discharged pressure. Also, due to the increased presence of rotating stall over the second surge cycle, the compressor starts to settle to an equilibrium value. After the entrance into the third surge cycle, the surge behavior disappears and the compressor is at a stalled, but stable operating point. Thus, the flow regime between rotating stall only and surge only is one of an equilibrating surge cycle, i.e., a surge cycle that decays to a stable equilibrium point.

At B = 0.76, a classic surge instability results. Figure 2c shows that steady flow exists up to 104 rotor revolutions, when a small stall cell emerges and rapidly grows into its full size in about 7 revolutions. For the next 11 rotor revolutions, the rotating stall cell stays relatively constant. At 134 revolutions, rotating stall quickly disappears and the compressor is unstalled until the plenum starts discharging again, with the cycle then repeating 1.5 more times. Note that unlike the rotating stall case or the modified surge cycle, the plenum pressure is able to charge up even higher than before the instability. The difference is that this process leads to a growing hysteresis loop on the performance map, i.e., the flow is not able to settle into a steady operating cycle. Also, there is no reverse flow, indicating that this is classic surge and not deep surge.

The compressor flow regime between rotating stall and classic surge is modified surge during which rotating stall persists throughout the surge cycle. At B = 0.26, rotating stall exists without any surge. At B = 0.40, the instability is characteristically surge, but a varying degree of rotating stall is present throughout the entire time. At B = 0.76, surge cycle exists without rotating stall, hence the difference between classic surge and modified surge. Figure 3 illustrates the range of B parameters in which the behavior typical of modified surge exists. Greitzer's[5] modified surge cycle would exist over B parameter range of 0.65–1.0. Jun et al.[7] had modified surge cycles over a B range of 0.75–1.8. The broadness of B parameters through which modified surge occurs indicates the importance of this intermediate flow regime.

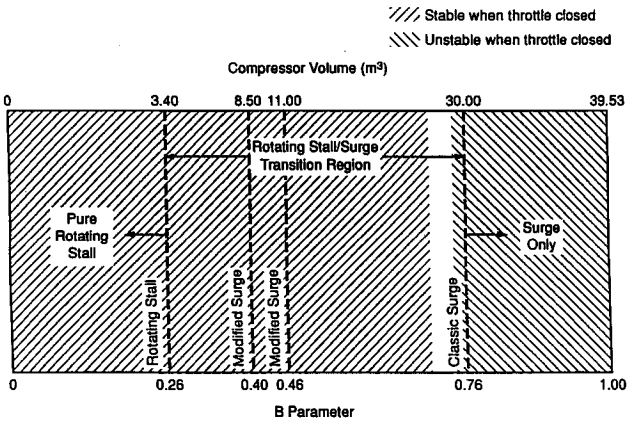

Fig. 3 Compressor instability modes.

DFT Analysis Frequencies

Since the DFT analysis of the unsteady pressure response takes the first harmonic of one cycle of data of a known period or frequency, it is absolutely essential that the specified frequency for the DFT analysis be as accurate as possible to minimize leakage errors. The Gabor transform is used to generate the Gabor spectrogram from which the characteristic rotating stall and surge frequencies are identified. Figure 4 shows the Gabor spectrogram for the first-stage rotor blade row, leading-edge suction surface pressure transducer for the instability modes. The vertical axis represents time and the horizontal axis is frequency. Thus, the rise and fall of important frequencies in the unsteady pressure response are shown by the intensity of the pressure magnitude. Since the pressure transducers are mounted on the rotor blading, the rotating stall cell speeds are relative to the rotor. However,

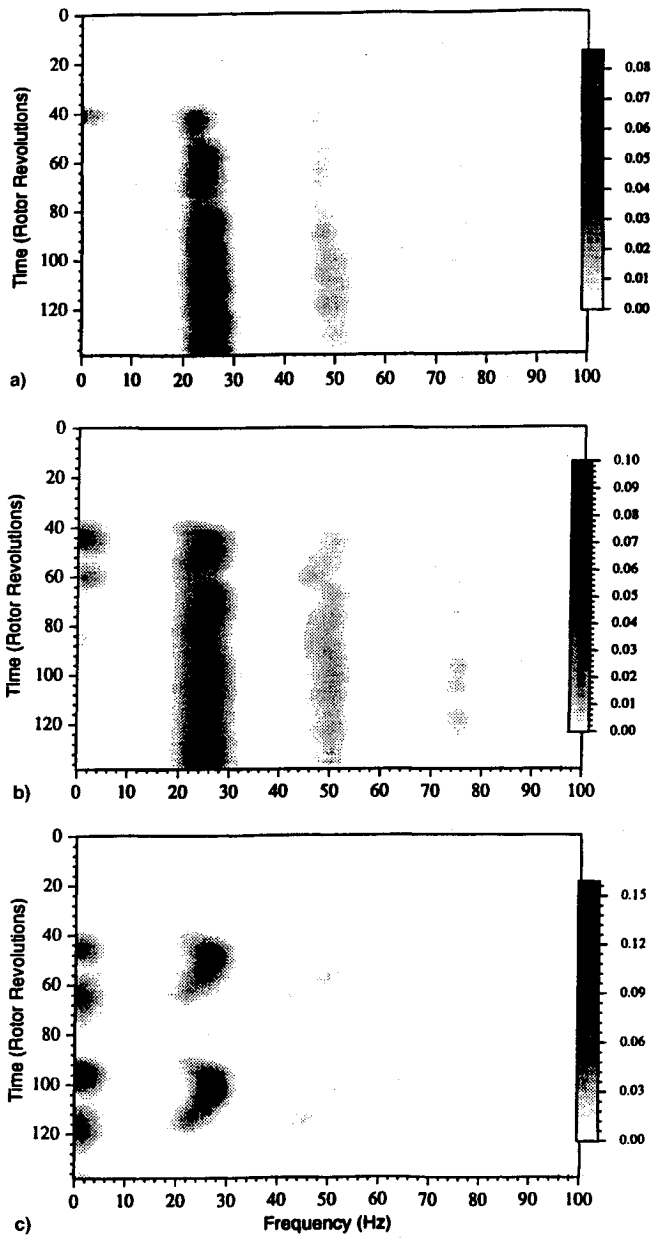

Fig. 4 Gabor spectrogram of suction surface leading-edge pressure response to instability modes: a) pure rotating stall (B = 0.26), b) modified surge close to pure rotating stall (B = 0.40), and c) classic surge (B = 0.76).

since surge is not a circumferential flow phenomena, the surge frequencies identified by the Gabor spectrogram are the same in the rotating and absolute reference frames.

Figure 4 reveals that the relevant rotating stall frequencies emerge at approximately 100 rotor revolutions. At B = 0.26, rotating stall undergoes three frequency changes, from 21.9 (15.6 Hz absolute) to 23.4 Hz (14.1 Hz) to 24.7 Hz (12.8 Hz) to 25 Hz (12.5 Hz). The dominant frequency is 24.2 Hz with variations less than 10%. For B = 0.4, the relevant frequencies are the surge frequency, 1.17 Hz, and the rotating stall frequency of 24.6 Hz (12.9 Hz). Unlike the pure rotating stall case, the stall frequency changes less than 1.6% during the modified surge cycle. At B = 0.76, the surge frequency is 0.75 Hz and the dominant rotating stall frequency is 25.8 Hz, with the variations less than 15%. Note that the surge frequencies were approximately calculated from the time elapsed between each surge cycle rather than from the Gabor spectrogram because of the poor frequency resolution of the spectrogram, 0.8 Hz. Since the variations in the rotating stall frequency are within 20%, using the dominant frequency for the harmonic analysis yields errors in magnitude and phase of less than 10% and 40 deg, respectively.

Unsteady Aerodynamic Forcing Functions

The transient forcing function resulting from the rotating stall excitation at the various compressor instability modes are presented in Figs. 5–7. These forcing functions are the rotating stall frequency component of the total unsteady velocity. Each of these figures presents u^+ and v^+, $\bar{W}$, and the magnitude and phase of the streamwise-to-transverse gust ratio u^+/v^+.

The rotating stall forcing function for B = 0.26 is shown in Fig. 5. Until 100 rotor revolutions, the streamwise and transverse gust velocities are low, less than 5 ft/s, and the $\bar{W}$ is constant at approximately 119 ft/s. Instability is encountered at 100 rotor revolutions, with v^+ increasing to approximately 20 ft/s in 1 rotor revolution and remaining at this level. In contrast, u^+ increases linearly with time, while $\bar{W}$ local to the 24.2-Hz stall cell decreases linearly.

Before the onset of the instability, times less than 100 rotor revolutions, the magnitude and phase of u^+/v^+ undergo significant fluctuations. This is because no signal with the 24.2-Hz frequency is present, i.e., no rotating stall component. After the compressor encounters the rotating stall instability, the magnitude of u^+/v^+ initially fluctuates around a value of 0.6 for about 35 rotor revolutions, and the phase of u^+/v^+ changes from about 60 to 150 deg. After 135 rotor revolutions, the magnitude of u^+/v^+ increases linearly while the phase becomes constant at approximately 150 deg. Note that the magnitude of u^+/v^+ is greater than 1, and is increasing. This is in contrast to typical forced response gust component ratios for compressors in which u^+/v^+ is small or order one. The rotating stall excitation generating large values of u^+/v^+ is similar to the behavior observed by Kim and Fleeter[11] from separated flow forcing functions, i.e., rotating stall cell is a severely separated flow forcing function.

With B = 0.40 (Fig. 6) the results are similar to the pure rotating stall case, u^+ and v^+ are less than 5 ft/s for times less than 100 rotor revolutions. At 100 rotor revolutions, the modified surge instability is encountered, with both u^+ and v^+ increasing very rapidly in approximately 4 rotor revolutions to 45 ft/s and 25 ft/s respectively. v^+ then decreases to half-amplitude during the recovery phase of the first surge cycle, but reaches the previous magnitude level during subsequent modified surge cycles. In contrast, u^+ and $\bar{W}$ track the blow-down and recovery phases of the modified surge cycle. Note that the value of u^+ during the middle of each modified surge cycle is approximately the same, with a maximum value of approximately 45 ft/s.

The magnitude of u^+/v^+ follows the behavior of u^+ since the level of v^+ is nearly constant except during the recovery phase of the first modified surge cycle. Values of u^+/v^+ are greater than 1.0, becoming 2.5 during the core of the modified surge cycle where the flow is most stalled. Similar to B = 0.26, the phase of u^+/v^+ is approximately constant at 150 deg when large rotating stall cells are prevalent, but changes from/to 0 deg at the entrance and exit of the modified surge cycle where rotating stall is weak.

During the classic surge instability mode (Fig. 7), u^+, v^+, and $\bar{W}$ track the behavior of classic surge equally well because of the complete disappearance of rotating stall during the recovery phase of the surge cycle. The maximum magnitude of gust velocities are relatively unchanged from other instability modes, being approximately 45 and 23 ft/s for u^+ and v^+, respectively. This results in a u^+/v^+ magnitude ranging from 1.5 to 3.0 within the surge cycle, with the phase of u^+/v^+ being nearly constant at 150 deg in regions where rotating stall exists.

The transient forcing functions resulting from the surge excitation during the various instability modes are presented in Figs. 8 and 9. These define the surge frequency component of the total unsteady velocity, with u^+ and v^+, $\bar{W}$, and the

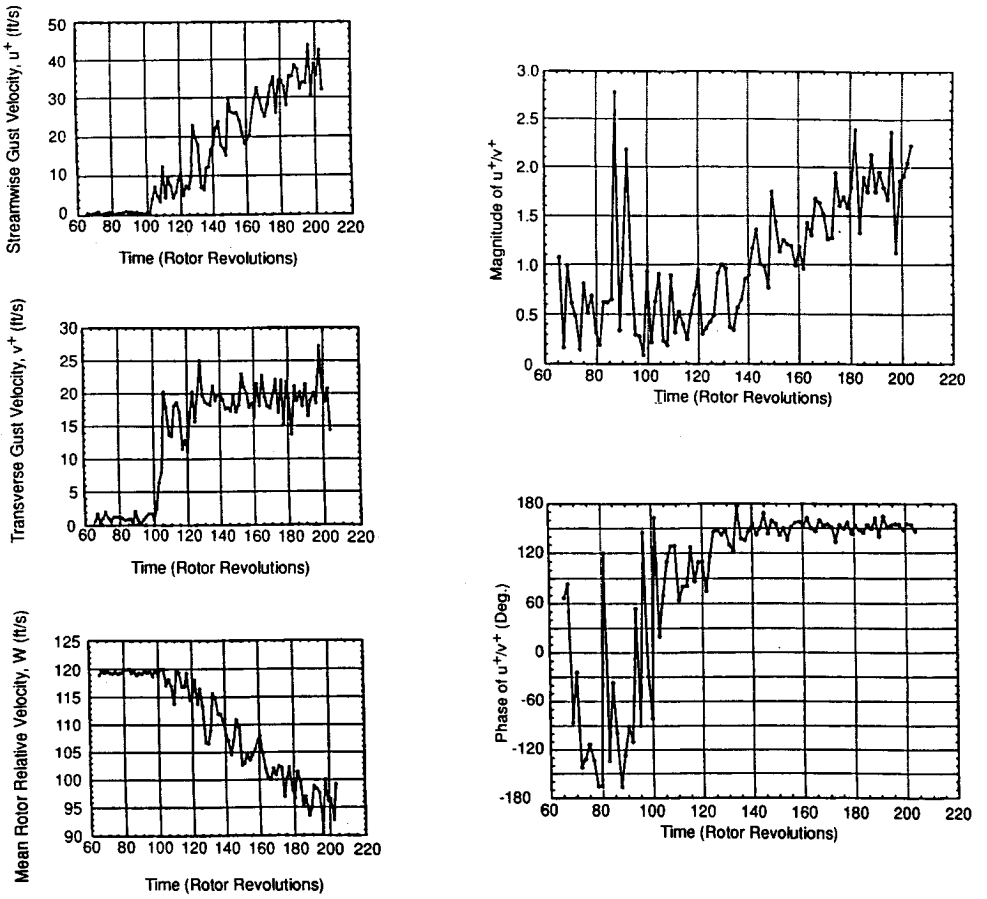

Fig. 5 Rotating stall forcing function during pure rotating stall (13.3- or 24.2-Hz rotating frame).

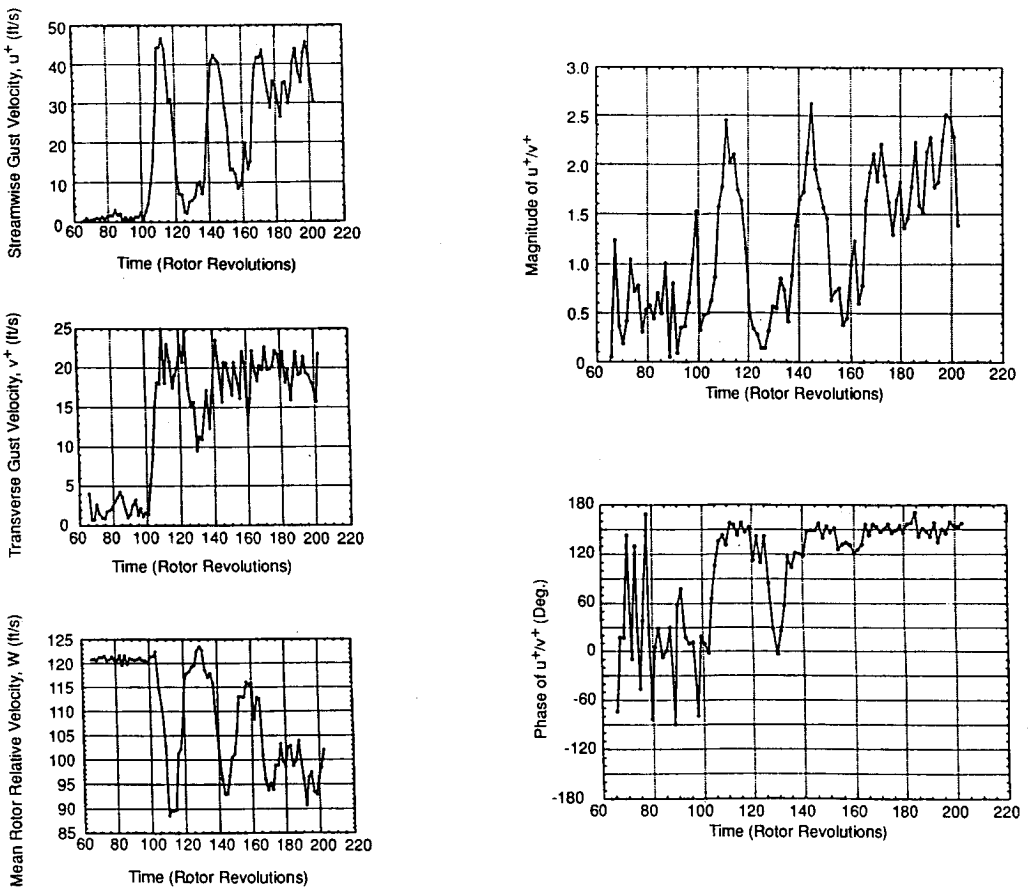

Fig. 6 Rotating stall forcing function during modified surge (12.9- or 24.6-Hz rotating frame).

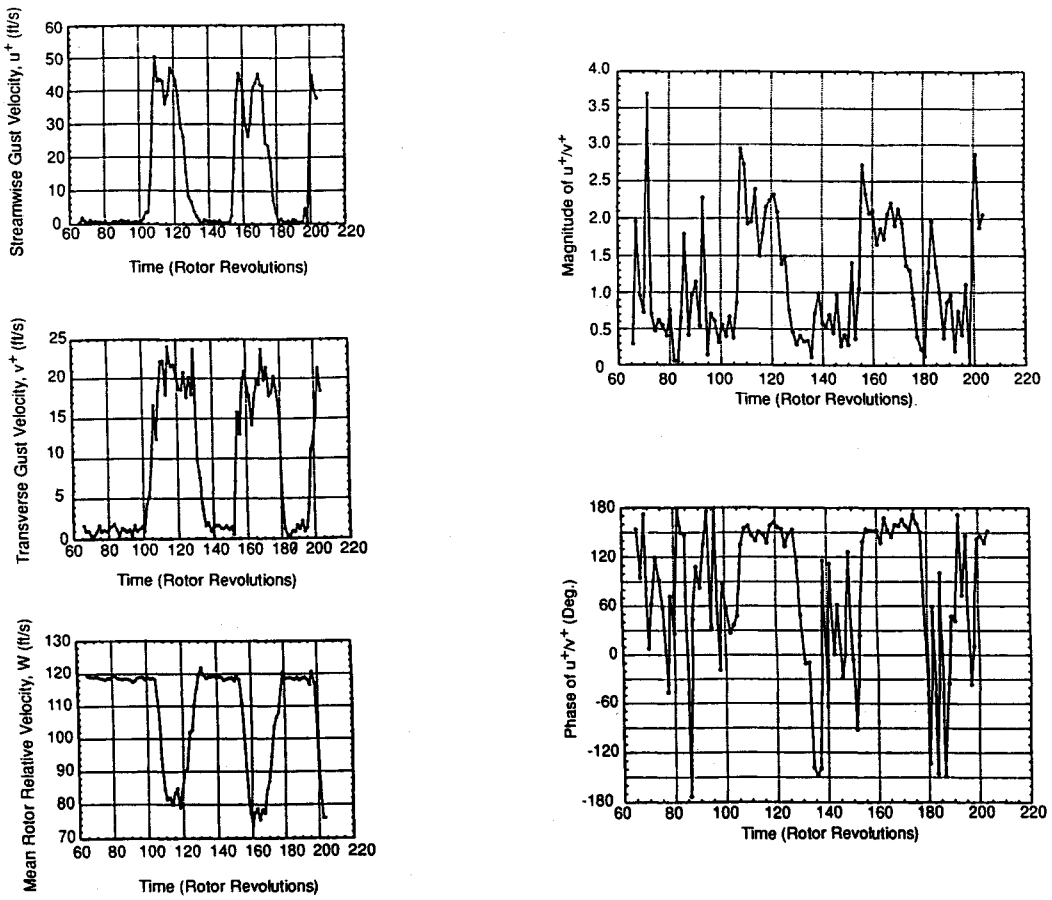

Fig. 7 Rotating stall forcing function during classic surge (11.7- or 25.8-Hz rotating frame).

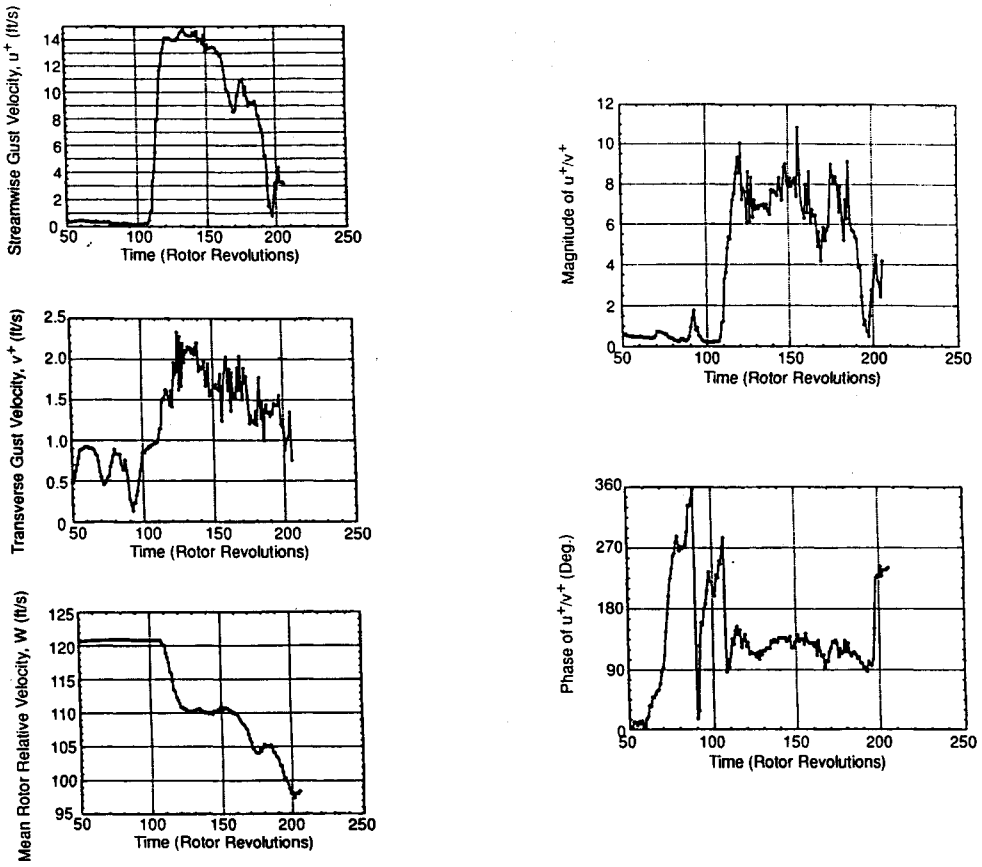

Fig. 8 Surge forcing function during modified surge close to pure rotating stall (1.17 Hz).

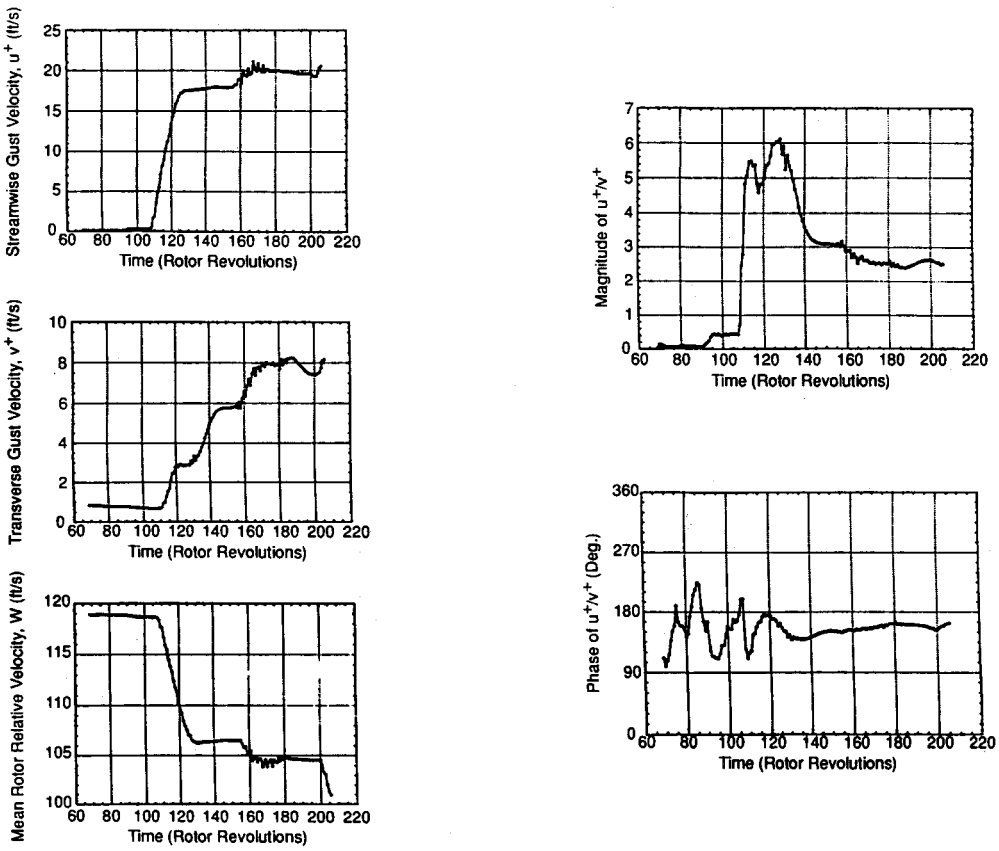

Fig. 9 Surge forcing function during classic surge (0.75 Hz).

magnitude and phase of u^+/v^+ presented. Note that since $B = 0.26$ corresponds to pure rotating stall, this case is not analyzed for the surge excitation or response.

The surge unsteady forcing function during modified surge close to pure rotating stall, $B = 0.40$, is shown in Fig. 8. Before the start of the modified surge cycle at approximately 110 rotor revolutions, u^+ and v^+ are small. Both then undergo a sudden and rapid increase. The increase in u^+ is particularly large, approximately 15 ft/s or 12% of the presurge $\bar{W}$. u^+ remains at this value until approximately 150 rotor revolutions, when it decreases, first by 2 ft/s and then by 5 ft/s to reach a relative minimum at 170 rotor revolutions. At this time, u^+ rapidly decreases to less than 5 ft/s. The first decrease u^+ corresponds to the point at which the modified surge cycle exhibits increased rotating stall during the recovery phase of the second modified surge cycle. The magnitude of u^+ continues to decrease as the rotating stall increases. In contrast, v^+ increases to a peak value of 2.3 ft/s and remains at this value until 140 rotor revolutions. It then decreases slowly to the presurge level of 1 ft/s.

Prior to 110 rotor revolutions, $\bar{W}$ is approximately constant at 121 ft/s. At the onset of the modified surge cycle $\bar{W}$ undergoes a sudden and rapid deceleration to 110 ft/s, which is then maintained during the core and exit of the modified surge cycle. During initiation into the second modified surge cycle $\bar{W}$ again starts to decrease to 105 ft/s. The decrease in $\bar{W}$ experienced during the second modified surge cycle is less because of the increasing presence of rotating stall, and hence the decrease in the surge component. Upon initiation into the third modified surge cycle $\bar{W}$ decreases further to approximately 97 ft/s.

The surge excitation forcing function is also presented as the u^+/v^+ ratio in Fig. 8. Since both u^+ and v^+ are changing during the onset and development of the modified surge cycle, u^+/v^+ also changes with time. Approximately 20 rotor revolutions prior to the onset of the instability there is a small peak in the magnitude of u^+/v^+. At instability onset the magnitude of u^+/v^+ increases rapidly to 10 in approximately 10 rotor revolutions, and fluctuates between 4–11 during the development of the modified surge cycle. At the end of 200 rotor revolutions the magnitude of u^+/v^+ is small because u^+ is at its low presurge levels.

The phase of u^+/v^+ provides information about the presence of surge. Prior to the start of the modified surge cycle, the phase is constantly changing. However, at instability onset, the phase changes by 180 deg from the pre-modified surge value and stays at a constant level of approximately 140 deg. Toward the end of the measurement period, near 190 rotor revolutions, the phase of u^+/v^+ undergoes a large change due to the disappearance of the surge cycle.

In the classic surge mode, $B = 0.76$, the temporal trends found in the modified surge excitation are much more pronounced (Fig. 9). u^+ increases rapidly to about 18 ft/s at instability onset and remains at this value until the second surge cycle is encountered, where u^+ further increases to 20 ft/s. This second velocity increase is due to the classic surge cycle growing in size with time. Similarly v^+ is small until the onset of the instability, then increases rapidly to a new value with each surge cycle. The transition to a new value occurs at the entrance and the exit of the surge cycle. Note the significant increase in the magnitude of v^+ in comparison to the values during the modified surge cycles: 6 ft/s after the first cycle, 8 ft/s after the second cycle. $\bar{W}$ decreases where u^+ increases, and increases where u^+ decreases.

The magnitude and phase of u^+/v^+ are also shown in Fig. 9. Note the slight increase in the magnitude before surge initiation, at approximately 90 revolutions. This presurge increase is different from the modified surge case in that it does not exhibit a peak value. At surge initiation, the magnitude increases almost instantaneously to 5.5, staying near 5.5 until approximately 130 rotor revolutions. It then starts to decrease rapidly until about 140 revolutions, when the decrease slows and settles to about 2.6. The phase of u^+/v^+ undergoes a slight oscillation for about 20 revolutions during the time frame

that the magnitude rises and falls. At approximately 140 revolutions, the phase settles to approximately 160 deg.

The surge forcing functions are similar to the rotating stall forcing function in several ways. u^+ and $\bar{W}$ follow the transient flow behavior of rotating stall, the modified surge, and classic surge cycles. Also, the level of u^+ is fairly constant regardless of the instability mode, being about 50 ft/s for rotating stall and 15–20 ft/s for surge. However, v^+ differs in magnitude between the rotating stall and surge excitations. The rotating stall-generated v^+ is approximately constant regardless of the instability mode. The surge-generated v^+ magnitude changes with instability mode, being lowest for $B = 0.40$, with a peak value of 2.3 ft/s, and largest for $B = 0.76$, having a peak value of about 8 ft/s. The ratio u^+/v^+ for both the rotating stall and surge forcing functions are similar in that the transient behavior tracks the instability behavior in general, but differ in magnitude. The rotating stall excitation results in a lower magnitude u^+/v^+ less than 3, while the surge excitation has u^+/v^+ ranging from 4 to 14.

Unsteady Aerodynamic Response

The first-stage rotor blade complex unsteady lift for the instability modes are shown in Fig. 10. The magnitude specifies the blade response to rotating stall since the frequencies selected for the DFT analysis described earlier are the rotating stall frequencies. The coherence of the unsteady lift indicates the presence of a physical wave, i.e., the rotating stall.

With the rotating stall excitation, the unsteady lift is very low until just before 100 rotor revolutions when the blade suddenly responds to the rotating stall, with the magnitude very rapidly increasing from 0.0025 to 0.017 psi in approximately 10 rotor revolutions. Then the rotor responds to the growth in stall cell depth, with the magnitude increasing slowly from 0.017 to 0.0275 psi. These trends correspond to the time history of v^+ due to rotating stall excitation (Fig. 5). At the same time that the unsteady lift magnitude sharply increases, the phase becomes coherent, which indicates stall cell propagation. From about 100–160 rotor revolutions, the phase decreases, showing that the actual rotating stall wave is slower than the specified frequency of 24.2 Hz (13.3 Hz). The actual speed at rotating stall inception is 21 Hz (17 Hz) per Eq. (2).

With $B = 0.40$, rotating stall excitation during modified surge, the approximately 1.5 cycles of surge becoming rotating stall is reflected in the development of the unsteady lift. Until approximately 100 rotor revolutions, the unsteady lift magnitude is low, approximately 0.002 psi. Then, the blade row responds to the rotating stall cell excitation in the first surge cycle and the unsteady lift increases very rapidly to its peak value during the next 15 rotor revolutions. Then, the unsteady lift magnitude decreases during the compressor recovery period of the first surge cycle and reaches the local minimum unsteady lift of 0.015 psi at about 125 rotor revolutions. It then undergoes two more small fluctuations, settling to a magnitude of 0.0275 psi. These fluctuations correspond to the fluctuations in the rotating stall v^+ (Fig. 6). At approximately 100 rotor revolutions, the phase starts to become coherent, with the phase slope being negative corresponding to a speed of 23 Hz (14 Hz). At approximately 115 rotor revolutions, the phase becomes flat, indicating that the stall speed is 24.6 Hz (12.9 Hz). During the recovery period of the first modified surge cycle, the stall speed is approximately 22.9 Hz (14.6 Hz). During the second modified surge cycle peak, at 140 rotor revolutions, the stall speed is again 24.6 Hz. From the recovery period of the second surge cycle and the settling into a steady stalled operating loop, the stall speed changes from 24.2 (13.3) to 24.7 Hz (12.8 Hz). The phase stays coherent during the recovery zone of the modified surge cycle because rotating stall is present throughout the entire modified surge cycle.

The rotating stall excitation complex unsteady lift during the classic surge cycle is presented in Fig. 10c. Analogous to the v^+ magnitude of Fig. 7, the time history of the unsteady lift magnitude clearly shows the nature of the classic surge cycle. It increases very rapidly and suddenly at 100 rotor revolutions, reaching its peak value of 0.032 psi, and then decreases just as rapidly to its presurge level. This is in contrast to the blade row response to rotating stall during the modified surge cycle where v^+ and the unsteady lift magnitude did not fall to presurge levels because of the continued presence of rotating stall throughout the surge cycle. This difference between the modified and classic surge cycles is also evident in the unsteady lift phase data. The phase coherence during the rise and fall of rotating stall within the surge cycle is no longer present during the surge recovery periods. Within the surge cycle, the rotating stall speed changes from 23.5 (14) to 26.8 (10.7) to 23.5 Hz.

Figure 11 presents the magnitude of the unsteady lift on the first-stage rotor blade generated by a surge excitation for modified surge close to pure rotating stall at 1.7 Hz and classic surge at 0.75 Hz. The modified surge close to pure rotating stall cycle is initiated at approximately 100 rotor revolutions, with the unsteady lift magnitude increasing very sharply to 0.007 psi where there is a slight lull in growth. The magnitude then continues to rapidly increase until a maximum of 0.011 psi at the end of the first modified surge cycle. The increase in the magnitude and the time of maximum lift correspond

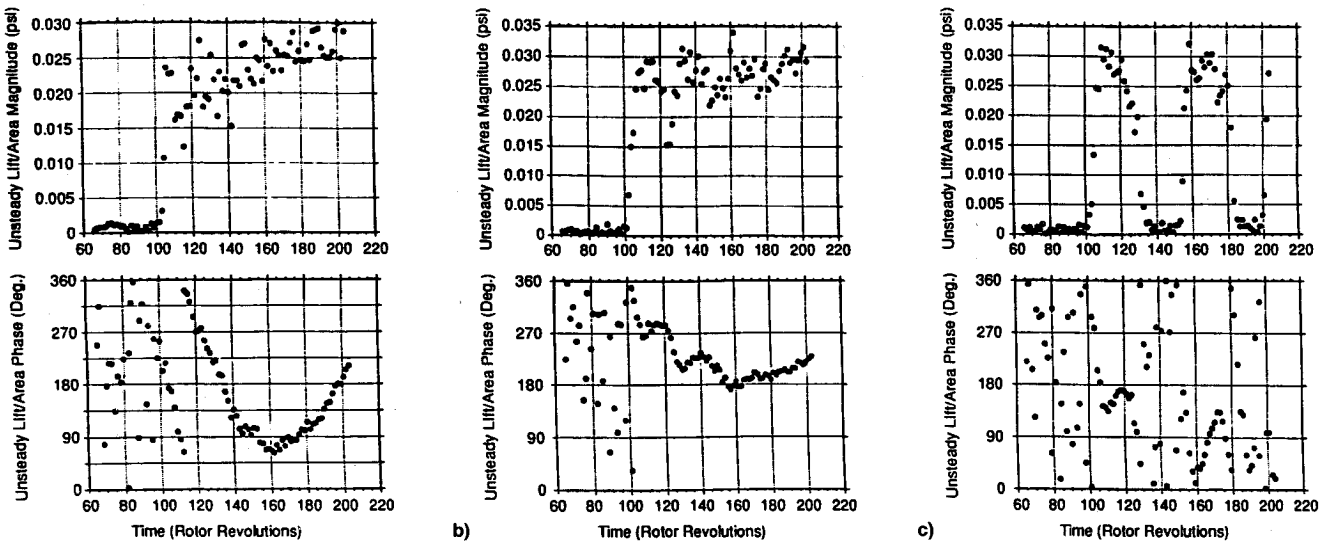

Fig. 10 Unsteady lift due to rotating stall excitation: a) pure rotating stall ($B = 0.26$), b) modified surge close to pure rotating stall ($B = 0.40$), and c) classic surge ($B = 0.76$).

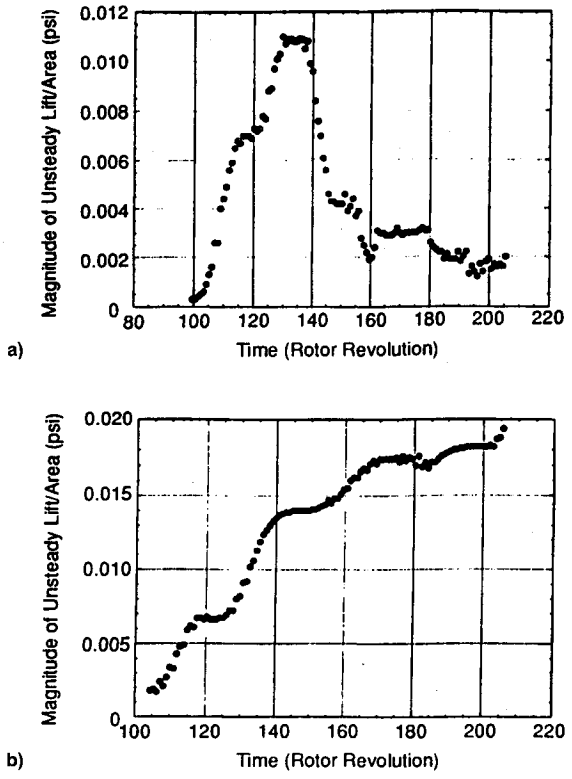

Fig. 11 Unsteady lift due to surge: a) modified surge close to pure rotating stall, $B = 0.40$ (1.17 Hz) and b) classic surge, $B = 0.76$ (0.75 Hz).

to the transient behavior of v^+. The decrease in the surge-generated unsteady lift occurs because after the first modified surge cycle, the presence of rotating stall increases significantly with each modified surge cycle. Therefore, after 130 rotor revolutions, the magnitude decreases fairly rapidly until 140 rotor revolutions, when the decrease in magnitude is considerably slower, tracking the merging of surge characteristics with rotating stall.

For the classic surge cycle, the unsteady lift magnitude starts to increase at approximately 105 rotor revolutions, with the rate of increase initially similar to the two modified surge cases. However, in contrast to the modified surge case, the unsteady lift does not decrease. Instead, it continues to increase, in correspondence with the v^+ time history.

In summary, the rotor blade unsteady lift generated by the surge excitation is dependent on the instability mode, because v^+ depended on the instability mode. The unsteady lift magnitude tends to be larger with the classic surge cycle than with the modified surge cycle due to the increased presence of rotating stall in the modified surge cycle. Also, since the modified surge cycle transforms into rotating stall, the unsteady lift magnitude reaches a maximum and then decreases, whereas the classic surge excitation does not attain a maximum unsteady lift.

Summary and Conclusions

The compressor unsteady aerodynamic forcing function and resulting unsteady aerodynamic response to rotating stall and surge excitation during the various compressor instability modes was experimentally investigated in a 3-stage axial flow research compressor. The forcing function was measured with a rotating cross hot-wire probe, with the resulting first-stage rotor blade response measured with blade surface mounted dynamic pressure transducers. Different compressor instability modes were generated by varying the compressor volume with the compressor operating at a constant rotational speed.

The rotating stall forcing function is characterized by a large u^+ that tracks the behavior of the compressor instability mode, increasing during the pure rotating stall mode, and increasing and decreasing during the modified surge and classic surge modes. In contrast, v^+ increases very abruptly at instability onset, then remains nearly constant except where the level of rotating stall is very low. In addition, the u^+/v^+ ratio is large.

The surge forcing function is characterized by a large u^+ component that tracks the compressor instability behavior. It increases at surge initiation and then either decreases due to the decreased surge content and increased rotating stall content, or increases in the classic surge case since this surge cycle becomes deeper. v^+ is dependent on the particular instability mode, increasing with increasing B value or decreased rotating stall component. The u^+/v^+ ratios are an order of magnitude larger than those due to rotating stall, indicating that surge is a severely separated flow forcing function to the blade row.

The unsteady aerodynamic lift reflects the basic behavior of rotating stall, increasing continuously during the pure rotating stall and increasing and decreasing accordingly during modified surge and classic surge modes. The maximum rotating stall unsteady lift, approximately 27% of the rotor blade steady lift just before instability onset, was independent of the instability mode. In contrast, the surge unsteady lift showed strong dependence on the instability mode, but the magnitude showed considerably less.

Acknowledgments

Research was sponsored by the Air Force Office of Scientific Research (AFSC) under Grant 91-0251. The United States Government is authorized to reproduce and distribute reprints for governmental purposes notwithstanding any copyright notation hereon.

References

[1]Haupt, U., Abdel-Hamid, A. N., Kaemmer, N., and Rautenberg, M., "Excitation of Blade Vibration by Flow Instability in Centrifugal Compressor," American Society of Mechanical Engineers Paper 86-GT-283, June 1986.

[2]Jin, D., Haupt, U., Hasemann, H., and Rautenberg, M., "Excitation of Blade Vibration Due to Surge of Centrifugal Compressor," American Society of Mechanical Engineers Paper 92-GT-149, June 1992.

[3]Jin, D., Haupt, U., Hasemann, H., and Rautenberg, M., "Blade Excitation by Circumferentially Asymmetric Rotating Stall in Centrifugal Compressors," American Society of Mechanical Engineers Paper 92-GT-148, June 1992.

[4]Greitzer, E. M., "Surge and Rotating Stall in Axial Flow Compressors, Part I: Theoretical Compression System Model," *Transactions of the American Society of Mechanical Engineers*, Vol. 98, April 1976, pp. 190–198.

[5]Greitzer, E. M., "Surge and Rotating Stall in Axial Flow Compressors, Part II: Experimental Results and Comparison with Theory," *Journal of Engineering for Power*, Vol. 98, April 1976, pp. 199–217.

[6]Pust, L., "Modified Surge in an Axial Flow Compressor," American Society of Mechanical Engineers Paper 92-GT-59, June 1992.

[7]Jun, H., Cai, T. G., and Min, Z. H., "An Investigation of Post Stall Transients and Recoverability of Axial Compression Systems: Part I—A Simplified Method," American Society of Mechanical Engineers Paper 92-GT-55, June 1992.

[8]Garnier, V. H., Epstein, A. H., and Greitzer, E. M., "Rotating Waves as a Stall Inception in Axial Compressors," *Journal of Turbomachinery*, Vol. 113, April 1991, pp. 290–302.

[9]Hah, C., and Lakshminarayana, B., "Effect of Rotation on a Rotating Hot-Wire Sensor," *Journal of Physics, E: Scientific Instrumentation*, Vol. 11, 1978, pp. 999–1001.

[10]Day, I. J., "Axial Compressor Performance During Surge," AIAA Paper 91-7098, June 1991.

[11]Kim, K. H., and Fleeter, S., "Compressor Blade Row Unsteady Aerodynamic Response to Attached and Separated Flow Forcing Functions," AIAA Paper 92-0147, Jan. 1992.